Talanta 232 (2021) 122448

Contents lists available at ScienceDirect

Talanta

journal homepage: www.elsevier.com/locate/talanta

One-step colorimetric detection of *Staphylococcus aureus* based on target-induced shielding against the peroxidase mimicking activity of aptamer-functionalized gold-coated iron oxide nanocomposites

Huiwen Zhang, Shuo Yao, Xiuling Song, Kun Xu, Juan Wang, Juan Li *, Chao Zhao **, Minghua Jin ***

School of Public Health, Jilin University, Changchun, 130021, China

ARTICLE INFO

Keywords:
Food safety
Foodborne pathogen
Visual detection
Fe3O4/Au nanocomposites
shielding action

ABSTRACT

Staphylococcus aureus (*S. aureus*) is one of the most threatened food-borne pathogens. Thus, it is necessary to establish fast, portable and reliable tools to realize the identification of *S. aureus*. Herein, the authors describe an effective colorimetric-based biosensor for the detection of *S. aureus* in multiple types of samples. Initially, a nanozyme composed of gold and iron oxide nanoparticles was synthesized and further modified with *S. aureus*-specific aptamer via Au–S bond. By utilizing the intrinsic peroxidase-like activity of the above magnetic conjugates, 3,3′,5,5′-tetramethylbenzidine (TMB) can be transferred to oxTMB by oxidation of hydrogen peroxide (H_2O_2), resulting in a visible blue color. However, the introduction of *S. aureus* can turn off the UV–vis absorbance signals of TMB-H_2O_2 system, due to the identification property of the nanozyme probe. Consequently, the optical density of the mixed solution measured at 652 nm decreased linearly as the concentration of *S. aureus* increased from 10 to 10^6 CFU mL^{-1}, with the visible limit of detection as low as 10 CFU mL^{-1}. The as-prepared sensor can detect *S. aureus* in spiked water, milk and urine samples quantitatively during 12 min without any pre-enrichment, separation or washing steps. In our perception, the one-step colorimetric assay show promise in practical on-site detection of *S. aureus*.

1. Introduction

Staphylococcus aureus (*S. aureus*) is a facultative anaerobic and Gram-positive coccus [1], which is widely distributed and spread through air, water and food. *S. aureus* emerged as one of the most significant food-borne pathogens threatening human health since it can cause a variety of diseases, ranging from mild skin and soft tissue infections, food poisoning to life-threatening diseases such as pneumonia, endocarditis, osteomyelitis, sepsis, scalded skin syndrome and toxic shock syndrome [2–4]. In addition, *S. aureus* possesses various virulence factors and can develop multiple resistances to antimicrobial agents, leading to a dramatic increase in the risk of infection [5]. Therefore, the detection of *S. aureus* has become an important research topic in food safety and public health.

For the past few decades, bacterial culture and colony counting has still been considered as the gold standard for detecting *S. aureus*, even though it was time-consuming, cumbersome to operate, and high demands on the operator and the laboratory environment, wasting valuable time of patients with serious bacterial infections [6]. Nucleic acid detection strategies such as real-time quantitative polymerase chain reaction (qPCR) have attracted considerable attention, not only because it can significantly shorten the analysis time, but also because it can amplify target regions of the bacterial genome exponentially within a few hours, making it more selective and sensitive. However, the DNA polymerase used in PCR is easily inhibited by matrix-related factors in a variety of samples and the results of PCR may be unreliable when low levels of the target bacteria are present in large volume samples [7]. In addition, PCR-based assays are not suitable for on-site detection due to their high instrumentation and reagent handling requirements [8].

Currently, immunological detection technologies rely on the high specificity of antigen-antibody reactions to achieve rapid and accurate detection [9]. More importantly, aptamers, as short RNA or

* Corresponding author.
** Corresponding author.
*** Corresponding author.
E-mail addresses: li_juan@jlu.edu.cn (J. Li), czhao0529@jlu.edu.cn (C. Zhao), jinmh@jlu.edu.cn (M. Jin).

https://doi.org/10.1016/j.talanta.2021.122448
Received 3 January 2021; Received in revised form 4 April 2021; Accepted 18 April 2021
Available online 1 May 2021

single-stranded DNA oligonucleotides, have attracted a great deal of attention as an alternative to antibodies since their discovery in the late 1990s [2], which can fold freely into unique three-dimensional conformations once they bind to the targets [10]. Compared to antibodies, aptamers offer numerous advantages, such as ease of large-scale chemical synthesis, amenability to modification, and resistance to denaturation and degradation [11]. Therefore, a number of bacterial-specific aptamers [2,12–15] have been selected and used for bacterial identification in combination with different amplified output signals, such as colorimetry [16], fluorescence [17], chemiluminescence [18], Raman scattering [19] and surface plasmon resonance [20]. Among these methods, the colorimetric method has been widely used in the field of on-site detection due to its operational convenience, simplicity, speed, and portability.

In order to overcome the disadvantages of natural enzymes such as high-cost and low stability under harsh environmental conditions [21], an important recent development in colorimetric sensors is the increasing use of nanozyme [22]. In contrast to many nanomaterials with intrinsic peroxidase-like activity, such as manganese dioxide nanorods [23], gold nanoparticles [24] and copper sulfide nanocubes [25], ferroferric oxide nanoparticles (Fe_3O_4 NPs), as a typical transition metal oxides, have received tremendous attention due to its outstanding peroxidase-like activity, low-cost, and non-toxicity [26, 27, 28]. Furthermore, their catalytic performance can be substantially improved by coating metal catalysts on the surface of magnetic nanoparticles to form hybrid nanocomposite [21,29]. These artificial enzymes catalyze the oxidation of 3,3′,5,5′-tetramethylbenzidine (TMB) and 2,2′-azino-bis (3-ethylbenzothiazoline-6-sulfonic acid) (ABTS) to produce colored products in the presence of hydrogen peroxide (H_2O_2), which has been successfully used to detect H_2O_2 [30], ascorbic acid [21], alkaline phosphatase [22], etc.

Inspired by the above considerations, this study aims to establish a fast and robust one-step colorimetric method for the detection of *S. aureus*. Fig. 1 illustrates the entire process of the proposed *S. aureus* detection method. Fe_3O_4 nanoparticles with strong peroxidase-like activity were firstly synthesized by co-precipitating method, and then decorated with gold nanoparticles via *in-situ* reduction method. To identify the target, the thiol-modified *S. aureus*-specific aptamer were conjugated to the as-prepared Fe_3O_4/Au nanocomposites by Au–S bonds [31]. Upon addition of *S. aureus*, the apt-Fe3O4/Au nanocomposites preferentially bind to the surface of the bacteria, resulting in the shielding of their catalytically active sites. With the addition of H_2O_2, the catalytic oxidation of TMB by nanocomposites was inhibited, then the blue product was formed and generated the lighter color. The color change from dark blue to light blue is the result of a decrease in catalytic activity proportional to the *S. aureus* concentration. Qualitative and quantitative analysis of *S. aureus* was achieved by visual and spectrophotometric measurements of different levels of the blue product. Importantly, our one-step method does not require any separation or washing procedures.

2. Experimental

2.1. Materials and reagents

Ferric chloride ($FeCl_3{\cdot}6H_2O$, 99%) were obtained from WWW.GUANGFUBIAOWU.COM (Tianjin, China) and Ferrous chloride ($FeCl_2{\cdot}4H_2O$, 99%) were obtained from Tianjin Guangfu Fine Chemical Research Institute (Tianjin, China). Hexadecyl trimethyl ammonium Bromide (CTAB) and 3,3′,5,5′-Tetramethylbenzidine (TMB) were purchased from Shanghai Macklin Biochemical Co.,Ltd. (Shanghai, China). Chloroauric acid ($HAuCl_4{\cdot}3H_2O$, 99%) were purchased from Alfa Aesar. Reagents such as Sodium hydroxide (NaOH) were all obtained from Beijing Chemical Reagent Co., Ltd., (Beijing, China). As previously reported [32], the 5′-thiol-modified DNA aptamer (5′SH-GCA ATG GTA CGG TAC TTC CTC GGC ACG TTC TCA GTA GCG CTC GCT GGT CAT CCC ACA GCT ACG TCA AAA GTG CAC GCT ACT TTG CTA A-3′) was selected for recognition of *S. aureus*, which provided by Sangon Biotech Co., Ltd. (Shanghai, China). Double-distilled water (ddH_2O) and phosphate-buffered saline (PBS, 0.01 M, pH 7.4) were home-made. All chemicals and reagents employed were of analytical grade and were used without any further purification.

2.2. Instruments

The UV–vis absorption spectra were measured with a spectrophotometer (TU-1810 DPC Persee, Beijing, China) using a 1 cm path-length quartz cell. Transmission electron microscopy (TEM) images of nanoparticles were performed on a JEOL JEM-2100F transmission electron microscope operated at an accelerating voltage of 200 kV (JEOL, Japan). Fourier transform infrared (FTIR) spectra in the region from 4000 to 500 cm^{-1} were recorded as KBr discs on a Nicolet 6700 FTIR spectrometer (Thermo Fisher Scientific, USA) for evaluating various encapsulated nanoparticles. The zeta potential measurements were determined using a zeta potential analyzer (NanoBrook 90 Plus Zeta, Brookhaven, USA).

2.3. Bacterial culture

All the bacterial strains used in this study were provided by the Department of Hygienic Inspection, School of Public Health, Jilin University (Changchun, China). With the exception of *Vibrio parahaemolyticusstrain* (*V. parahemolyticus*, ATCC17802) grown in Tryptone Soya Broth supplemented with 3.0% NaCl, *Staphylococcus aureus* (*S. aureus*, ATCC 25923), *Escherichia coli O157:H7* (*E. coli O157:H7*, ATCC 25922), *Listeria monocytogenes* (*L. monocytogenes*, ATCC 19111)

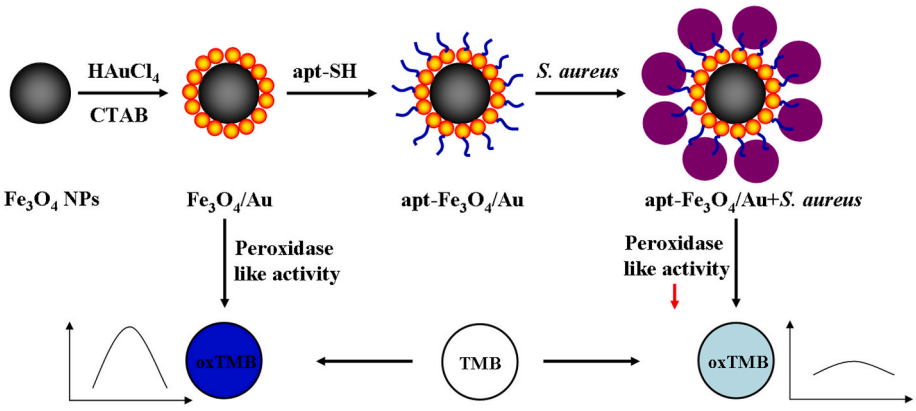

Fig. 1. Schematic diagram of the preparation technology for Fe_3O_4/Au nanocomposites and colorimetric detection of *S. aureus*.

and *Salmonella typhimurium* (*S. typhimurium*, ATCC 13311) were incubated in Luria-Bertani medium for 18 h at 37 °C with shaking at approximately 180 rpm. The concentrations of bacteria were determined on the standard plate count agar using the counting method. Inactive bacteria were obtained by incubating with 4% formaldehyde overnight at 4 °C and washing three times (3000 rpm, 15 min) with phosphate-buffered saline (PBS, pH 7.4). The suspensions of inactive bacteria diluted to different concentrations were stored at 4 °C.

2.4. Synthesis of Fe_3O_4/Au nanocomposites

The Fe_3O_4 NPs were manufactured by co-precipitating method according to an improved method for synthesizing MNPs-Au by Bozkurt A G [33]. Briefly, 3.46 g $FeCl_3{\cdot}6H_2O$ and 1.30 g $FeCl_2{\cdot}4H_2O$ were dissolved in 10 mL of ddH_2O and the solution was stirred at 350 rpm for 20 min until the color was clear and the solid was completely dissolved. Then 60 mL of 1 M NaOH was added dropwise into the mixture with continuous stirring at 350 rpm for 40 min. After that, the black precipitate was collected using a permanent magnet and washed several times with ddH_2O and 20 mL of 1 M $HClO_4$, respectively. After placing in an oven for 2 h at 37 °C, the precipitate was collected magnetically by washing three times with ddH_2O again. Finally, the products were dried in vacuum overnight at 60 °C. The dried Fe_3O_4 NPs were ground and stored at 4 °C.

To improve the catalytic performance of Fe_3O_4 NPs, the prepared Fe_3O_4 NPs were further decorated with gold nanoparticles by CTAB via in-situ reduction method. Typically, 0.02 g of Fe_3O_4 NPs were dissolved in 5 mL ddH_2O and sonicated for 10 min until the particles were uniformly dispersed. Then 5 mL of EDTA·2Na–NaOH mixture (1 g of EDTA·2Na dissolved in 10 mL of 1 M NaOH) was added to the Fe_3O_4 NPs solution and stirred at 350 rpm for 5 min. After removing the supernatant by magnetic separation, 7 mL of 0.1 M CTAB, 3 mL of 1% $HAuCl_4$ and 600 μL of 1 M NaOH were added in sequence. After stirring at 350 rpm for 5 min, 150 mg of hydroxylamine hydrochloride was added and stirred for another 5 min. After undisturbed placing at room temperature for 24 h, the black products were washed 3 times with ddH_2O, and resuspend into 10 mL solution. The 2 mg mL^{-1} Fe_3O_4/Au nanocomposites was obtained and stored at 4 °C for later use.

Synthesis of apt-conjugated Fe_3O_4/Au nanocomposites (apt-Fe_3O_4/Au nanocomposites).

The thiol-modified *S. aureus* aptamers were heated at 95 °C for 2 min, and then cooled to room temperature for activation. 1 mL of 2 mg mL^{-1} Fe_3O_4/Au nanocomposites was mixed with 10 μM aptamer (15 μL), then placed on a rotary mixer for 12 h 2 mg mL^{-1} apt-Fe_3O_4/Au nanocomposites were magnetically washed 3 times with ddH_2O, then resuspend in ddH_2O to 1 mL, and stored at 4 °C for later use.

2.5. The peroxidase-like activity of apt-Fe_3O_4/Au nanocomposites

Steady state kinetic measurements were conducted by monitoring the absorbance change at 652 nm with an ultraviolet–visible spectrophotometer in time-drive mode. Experiments were carried out using 0.15 mg mL^{-1} apt-Fe_3O_4/Au nanocomposites (100 μL) in 250 μL reaction buffer solution (0.2 M acetid acid (HAc)-sodium acetate (NaAc) buffer, pH = 4, room temperature) with 50 μL samples (*S. aureus* at concentrations of 10^6 CFU mL^{-1} or PBS buffer) in the presence of 42 mM TMB and 9800 mM H_2O_2 as substrate. The initial rates of the process were calculated using the molar absorption coefficient of the reaction product oxTMB ($\varepsilon_{652\ nm}$ = 39,000/(M*cm)). In order to display the kinetic characteristics, the velocity changes of the reaction were evaluated with changing concentrations of TMB by fixing the concentration of H_2O_2 (9800 mM), vice versa. The apparent kinetic parameters were estimated based on the Michaelis-Menten equation. The Michaelis-Menten constant was calculated using Lineweaver-Burk plots of the double reciprocal of the Michaelis-Menten equation, $1/v=(K_m/v_{max})\cdot(1/[S]) + 1/v_{max}$, where v is the initial velocity, v_{max} is the maximum reaction velocity, [S] is the substrate concentration, and K_m is the Michaelis constant.

2.6. Detection of *S. aureus*

The *S. aureus* stock solution was serially diluted into the following standard solutions (10–1 × 10^6 CFU mL^{-1}) using sterile PBS. After optimization of experimental conditions, each *S. aureus* standard solution (50 μL) was added into the colorimetric reaction system, which contained 100 μL of apt-Fe_3O_4/Au nanocomposites (0.15 mg mL^{-1}) and 90 μL HAc-NaAc buffer (pH = 4). Then the suspension was gently vortexed on a rotary mixer for 10 min. For the negative control, sterile PBS was used. Subsequently, 5 μL of 42 mM TMB and 5 μL of 9800 mM H_2O_2 were added in solution without any washing process. After reaction for 2 min at 37 °C, the spectrum in the range of 380–800 nm was recorded by an ultraviolet–visible spectrophotometer. Referring to the data processing process of Zhang [34] and Fu [35], the normalized absorbance value at 652 nm was calculated according to the following formula: $A_{norm} = (A_{652} - A_{min})/(A_{max} - A_{min})$. Among them, A_{norm} is the normalized absorbance value, A_{652} is the absorbance value at 652 nm, A_{max} and A_{min} are the maximum and minimum values in the series of data respectively.

2.7. Detection of *S. aureus* in real samples

To further investigate the potential practical applications of the method, multiple types of samples are selected as real sample models. Tap water, Nanhu Lake water and industrial wastewater were selected, in addition, urine samples were obtained from a hospital and milk samples were purchased from a local supermarket. These samples were firstly filtered for sterilization through 0.22 μm filter (Merck Millipore, USA), then *S. aureus* at concentrations of 10^2, 10^4, 10^6 CFU mL^{-1} was artificially inoculated into the pasteurized extract samples and detected using this detection protocol described in the previous section, except that PBS buffer was replaced with real samples.

3. Results and discussion

3.1. Characterization of the apt-Fe_3O_4/Au nanocomposites

To increase the catalytic activity of magnetic nanoparticles, gold nanoparticles as metallic catalyst was coated on Fe_3O_4 NPs by in-situ reduction method. The morphology characteristics and size distribution of synthesized nanocomposites are shown in Fig. 2, Fe_3O_4 NPs are uniformly distributed with an average size of 10.33 nm measured by Image J software. The size of Fe_3O_4/Au nanocomposites increases to 79.72 nm, which demonstrates that Fe_3O_4 NPs were decorated with gold to form Fe_3O_4/Au nanocomposites. Subsequently, the thiol-modified *S. aureus* aptamers were covalently linked to Fe_3O_4/Au nanocomposites via a gold-sulfur bond for specific identification of target bacteria, and the size of the probe increases to 96.83 nm. In addition, the results of particle size evaluation by DLS are shown in Fig. S1, compared to Fe_3O_4 NPs, the average size of Fe_3O_4/Au nanocomposites increases obviously from 44.72 nm to about 146.66 nm. Then the average diameter of apt-Fe_3O_4/Au nanocomposites increases to 299.07 nm after modification of the aptamer. To further confirm the successful immobilization of Au on Fe_3O_4 NPs, the EDS element map was used to characterize the distribution of different elements in the composites. As shown in Fig.S2, it could be observed that the main elements distributed on the surface of the material were Fe and Au, with the mass percentage of elements were 28.2 wt% and 71.8 wt% respectively.

As shown in Fig. 3a, the absorption peak of gold nanoparticles synthesized by sodium citrate reduction method is at 520 nm. When the gold nanoparticles are coated on Fe_3O_4 by in situ reduction method, the UV–visible absorption peak is red-shifted to 550 nm. The FTIR spectrum of Fe_3O_4 NPs, Fe_3O_4/Au nanocomposites and apt-Fe_3O_4/Au

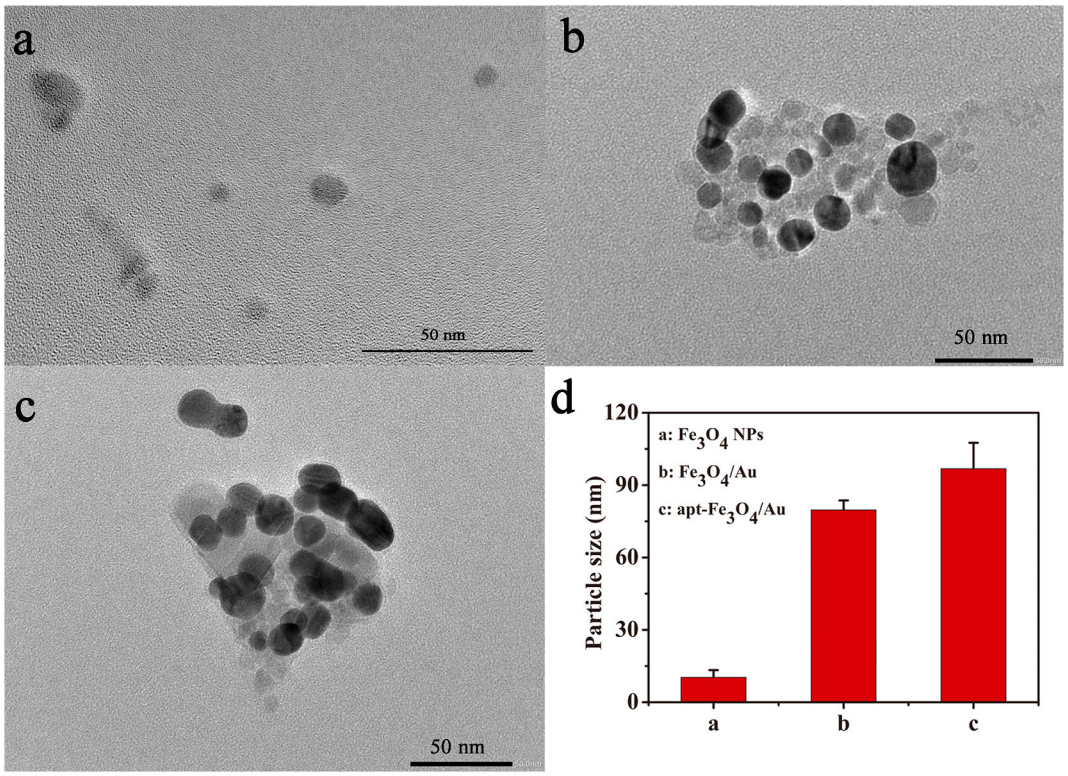

Fig. 2. TEM image of Fe_3O_4 NPs (a), Fe_3O_4/Au nanocomposites (b) and apt-Fe_3O_4/Au probes (c). d: Particle size distribution measured by Image J.

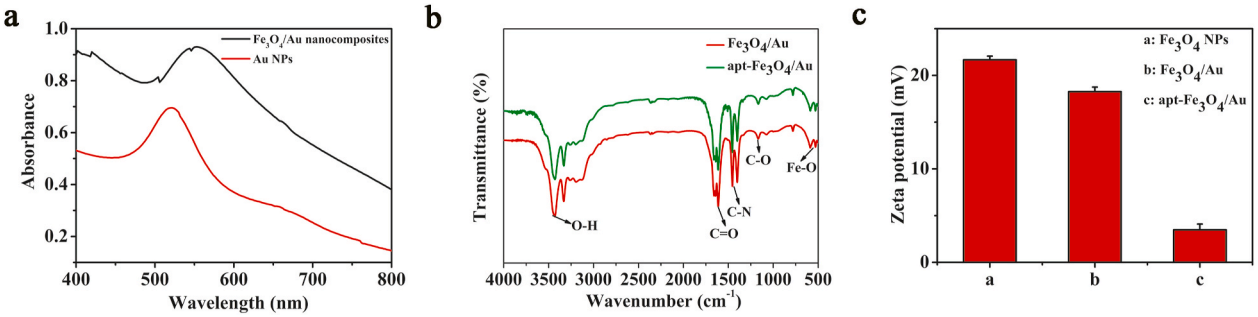

Fig. 3. a UV–Vis absorption spectra of Au NPs and Fe_3O_4/Au nanocomposites. **b** FT-IR spectra of Fe_3O_4/Au nanocomposites (red line) and apt-Fe_3O_4/Au nanocomposites (green line). **c** Zeta potential measurements of Fe_3O_4 NPs, Fe_3O_4/Au and apt-Fe_3O_4/Au nanocomposites. (For interpretation of the references to color in this figure legend, the reader is referred to the Web version of this article.)

nanocomposites is illustrated in Fig.3b and Fig.S3. The characteristic absorption peak located at 580 cm^{-1} can be attributed to the Fe–O stretch vibrations [36]. The absorption band at 1220, 1450, 1730 and 3400 cm^{-1} can be assigned to the stretching vibration of C–O bond, C–N bond, C═O bond and O–H bond, respectively [37]. The Zeta potential values of Fe_3O_4 NPs, Fe_3O_4/Au and apt-Fe_3O_4/Au nanocomposites were 21.67 ± 0.39, 18.26 ± 0.49 and 3.48 ± 0.62, respectively (Fig. 3c), the potential value decreases after coupling aptamer due to the electronegativity of naked DNA. The above results demonstrated that the aptamers were expectantly conjugated on the surface of Fe_3O_4/Au nanocomposites. Moreover, TEM image of *S. aureus* captured by apt--Fe_3O_4/Au nanocomposites is shown in Fig.S4, indicating that apt--Fe_3O_4/Au nanocomposites play a good role in enriching bacteria.

3.2. Validation of hypothesis

The peroxidase-like activity of the Fe_3O_4/Au nanocomposites was estimated by the catalytically oxidation of TMB by H_2O_2. When Fe_3O_4/Au nanocomposites was added to TMB in the presence of H_2O_2 (black line), significant absorption peak at 652 nm can be seen as in Fig. 4a. Fe_3O_4/Au nanocomposites had a good catalytic activity of peroxidation, because its shape provided sufficient active sites for catalytic oxidation of TMB. On the other hand, there were slight absorption peak variances in the absence of Fe_3O_4/Au nanocomposites (blue line). When *S. aureus* aptamers was covalently linked to Fe_3O_4/Au nanocomposites to form apt-Fe_3O_4/Au nanocomposites, the absorption peak at 652 nm was slightly decreased (red line), indicated that the catalytic activity of Fe_3O_4/Au was obscured by the aptamers. Furthermore, when bacteria were captured by apt-Fe_3O_4/Au nanocomposites, the absorption peak at 652 nm was further reduced, which proved that bacteria could mask the peroxidase-like catalytic activity of Fe_3O_4/Au nanocomposites (green line).

To demonstrate that our one-step method does not require any separation and washing procedures, we compared the absorption intensity results of magnetic cleaning twice and no washing step after apt-Fe_3O_4/Au nanocomposites captured *S. aureus*, as shown in Fig.S5. Student's *t*-

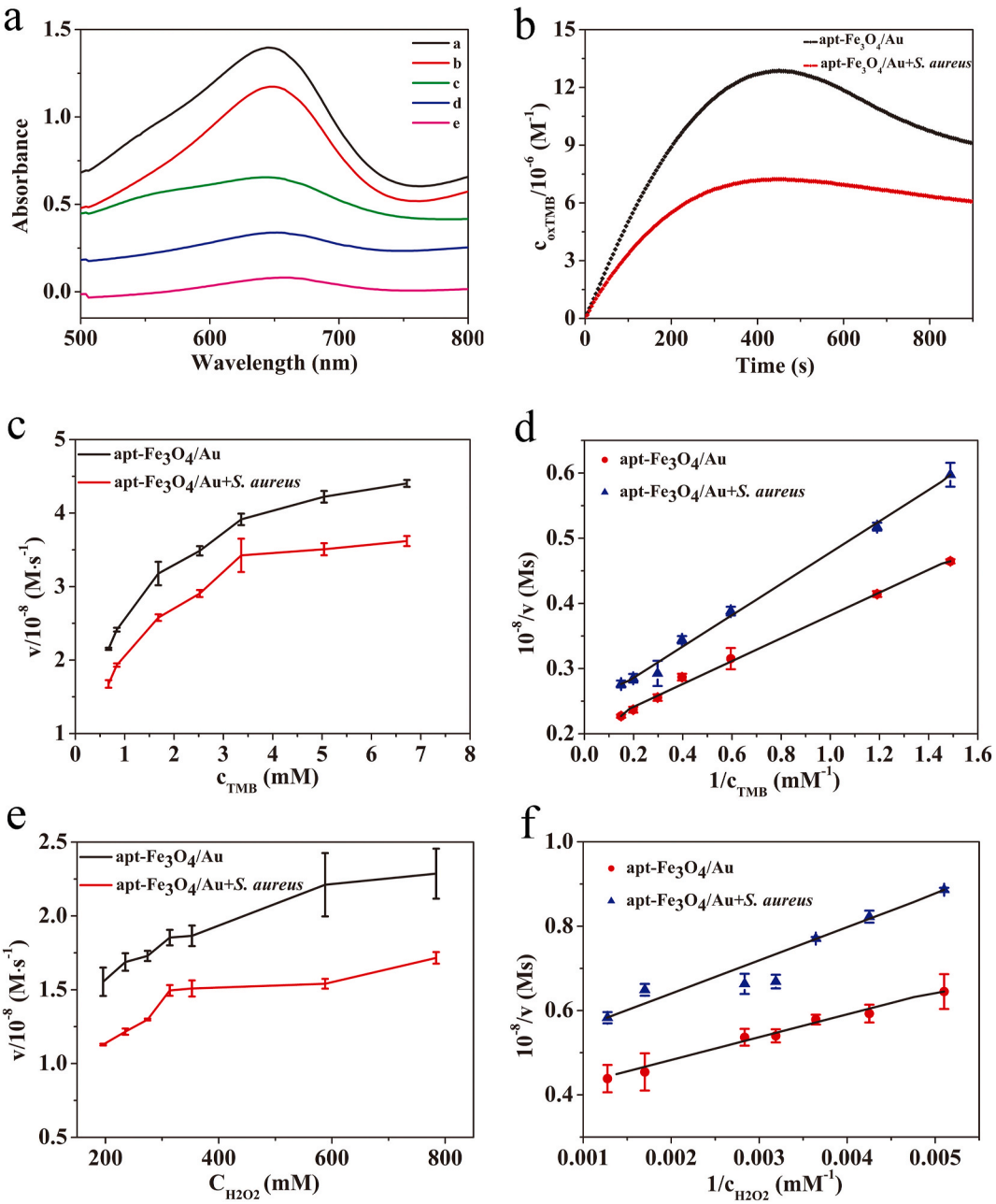

Fig. 4. a UV–Vis absorption spectra of different reaction systems (250 μL): Fe_3O_4/Au nanocomposites + TMB + H_2O_2 (a), apt-Fe_3O_4/Au nanocomposites + TMB + H_2O_2 (b), apt-Fe_3O_4/Au nanocomposites + *S. aureus* + TMB + H_2O_2 (c), TMB + H_2O_2 (d), *S. aureus* + TMB + H_2O_2 (e). Reaction conditions were Fe_3O_4/Au nanocomposites (0.15 mg mL^{-1}, 100 μL), apt-Fe_3O_4/Au nanocomposites (0.15 mg mL^{-1}, 100 μL), *S. aureus* (10^6 CFU mL^{-1}, 50 μL), TMB (42 mM) and H_2O_2 (9800 mM) at room temperature. **b** The time-dependent absorbance (at 652 nm) of apt-Fe_3O_4/Au nanocomposites (black line) and apt-Fe_3O_4/Au nanocomposites + *S. aureus* (red line). **c** Steady state kinetic assay of apt-Fe_3O_4/Au nanocomposites and apt-Fe_3O_4/Au nanocomposites + *S. aureus*. The concentration of H_2O_2 was 9800 mM and the TMB concentration was varied. **d** Double reciprocal plots of activity of apt-Fe_3O_4/Au nanocomposites and apt-Fe_3O_4/Au nanocomposites + *S. aureus* at a fixed concentration of H_2O_2 against differing concentration of TMB. **e** Steady state kinetic assay of apt-Fe_3O_4/Au nanocomposites and apt-Fe_3O_4/Au nanocomposites + *S. aureus*. The concentration of TMB was 42 mM and the H_2O_2 concentration was varied. **f** Double reciprocal plots of activity of apt-Fe_3O_4/Au nanocomposites and apt-Fe_3O_4/Au nanocomposites + *S. aureus* at a fixed concentration of TMB against differing concentration of H_2O_2. (For interpretation of the references to color in this figure legend, the reader is referred to the Web version of this article.)

test results showed no statistical difference between magnetic cleaning and without washing procedures. This indicates that our determination procedure can be achieved without washing. Then the storage stability of prepared Fe_3O_4/Au nanocomposites was investigated by detecting *S. aureus* (10^6 CFU mL^{-1}) using apt-Fe_3O_4/Au nanocomposites with different storage time. As shown in Fig.S6, the statistical analysis showed no statistical difference between fresh synthesized nanocomposites and the one stored for one year. This indicates that as prepared Fe_3O_4/Au nanocomposites has robust storage stability. As shown in Tab.S1, samples with concentrations of 100, 500 and 1000 CFU mL^{-1} were assayed with the established assay. The measured recoveries were in the range of 92.3–106.2 and the relative standard deviations were in the range of 3.9–12.3, indicating that the assay has good reproducibility.

3.3. Kinetic analysis of apt-Fe_3O_4/Au nanocomposites

The time-dependent absorbance (at 652 nm) of apt-Fe_3O_4/Au nanocomposites (black line) and apt-Fe_3O_4/Au nanocomposites with *S. aureus* (red line) are shown in Fig. 4b. The initial velocity of apt-Fe_3O_4/Au nanocomposites and apt-Fe_3O_4/Au nanocomposites with *S. aureus* were 0.5641×10^5 and 0.3590×10^5 M s^{-1}. This further proves the target-induced shielding effect due to the inhibition of catalytic activity of Fe_3O_4/Au by *S. aureus*.

Typical Michaelis-Menten curves (Fig. 4c, d, e, f and Tab.S2) are obtained in a certain range of TMB or H_2O_2 concentrations. With the Line weaverBurk equation, the associated enzyme kinetic parameters were firstly obtained at a fixed concentration of H_2O_2 against differing concentration of TMB. As shown in Tab.S1, Michaelis-Menten constant (K_m) and Maximum initial velocity (V_{max}) were 0.8502 mM, 0.4847×10^{-7} M s^{-1} for apt-Fe_3O_4/Au nanocomposites and 1.0097 mM, 0.4203×10^{-7} M s^{-1} for apt-Fe_3O_4/Au nanocomposites with *S. aureus*, respectively. Then the concentration of TMB was fixed at 42 mM, the K_m of apt-Fe_3O_4/Au nanocomposites increased from 147.2629 mM to 158.7519 mM with the increase of H_2O_2 in the absence and presence of target bacteria. K_m is a reflection of the affinity of enzyme for its substrate, and it is a very useful parameter by which the affinity of the catalyst for various substrates can be compared. The smaller the value of K_m, the more strongly the catalyst binds the substrate. Compared with the parameters of apt-Fe_3O_4/Au nanocomposites with *S. aureus*, K_m of apt-Fe_3O_4/Au nanocomposites was lower whereas V_{max} was higher. This indicated that the affinity between catalyst and substrate decreased after apt-Fe_3O_4/Au nanocomposites captured bacteria.

3.4. Optimization of experimental conditions

In order to obtain the optimal peroxidase catalytic activity of Fe_3O_4/Au nanocomposites, temperature and pH were optimized by investigating the absorbance of oxTMB at 652 nm and the results are shown in Fig.S7a,b. The value of absorbance increased with the increasing of temperature from 4 °C to 60 °C. However, the optimum growth temperature for live bacteria is around 37 ± 2 °C, that is commonly used temperature for bacterial culture and real sample testing in laboratory. Based on the above considerations, 37 °C was chosen as the optimal reaction condition catalyzed by Fe_3O_4/Au nanocomposites. Then the highest absorbance catalyzed by Fe_3O_4/Au nanocomposites was obtained at HAc-NaAc buffer when pH value was 4 (Fig.S7b). Subsequently, The concentration of apt-Fe_3O_4/Au nanocomposites and enrichment time were optimized by calculating relative activity (Relative activity = $(A_0\text{-}A)/A_0$, where A_0 and A are the absorbance of oxTMB at 652 nm in the absence and presence of *S. aureus*, respectively) (Fig. S7c,d). As the concentration of apt-Fe_3O_4/Au nanocomposites increased from 0.01 mg mL^{-1} to 0.15 mg mL^{-1}, the value of relative activity increased, while the concentration of apt-Fe_3O_4/Au nanocomposites increased above 0.15 mg mL^{-1}, the value of relative activity decreased. Therefore, the final concentration of 0.15 mg mL^{-1} of apt-Fe_3O_4/Au nanocomposites was used to reach the maximum relative activity. When apt-Fe_3O_4/Au nanocomposites were enriched *S. aureus* for 10min, the relative activity could reach 45%, and then within 20 min–120 min, the relative activity was stable at about 35%. Therefore, the most appropriate enrichment time was 10 min. In addition, the amount of TMB in the color reaction was optimized, as shown in Fig.S7e. When 5 μL of TMB (10 mg mL^{-1}) was added, the relative activity reached more than 20%, which was the optimal dosage for the reaction. On the basis of these results, subsequent experimental conditions were chosen to give the best results: (a) temperature: 37 °C; (b) pH = 4; (c) 0.15 mg mL^{-1} of Fe_3O_4/Au nanocomposites; (d) enrichment time: 10 min.

3.5. Sensitive detection of S. aureus

The performance of the colorimetric strategy was experimented under optimal assay conditions. The bare-eye limit of detection (LOD) for *S. aureus* was determined to be 10 CFU mL^{-1}. Then the instrument LOD was calculated according to the following formula: LOD = 3SD/slope. Where SD represents the standard deviation of negative control samples, and the slope was obtained from the fitted standard curve [38]. The detection limit of this assay was calculated to be 26 CFU mL^{-1}. As shown in Fig. 5a, the absorbance value is gradually decreased at 652 nm with increasing *S. aureus* concentration, revealing that *S. aureus* shield the peroxidase-like catalytic activity of Fe_3O_4/Au nanocomposites. The standard curve was plotted with the logarithm value of *S. aureus* concentration as the x-coordinate and the normalized absorbance value at 652 nm as the y-coordinate (Fig. 3b). The linear regression equation was $A_{norm} = -0.103\lg N + 0.623$, $R^2 = 0.995$, indicating that the established detection system had a good linear relationship. As shown in Tab.S3, compared with other methods reported in recent years for the detection of *S. aureus*, such as lateral flow assay, MNP-TiO_2-AP-SMCC-Biosensors or Chemiluminescence resonance energy transfer aptasensor, the detection system constructed in this study has a wider linear range and lower detection limit.

3.6. Specificity of the assay

To assess the specificity of the established assay, four common foodborne pathogens including *E. coli* O157:H7, *L. monocytogenes*, *V. parahemolyticus*, and *S. typhimurium* were selected for comparison with *S. aureus*, and the PBS sample was employed as negative control. As shown in Fig.6a, a remarkable decreased at 652 nm is observed in the presence of *S. aureus* alone and *S. aureus* mixed other interfering species, compared to those of the negative groups. Further, Fig. 6b shows that the normalized absorption intensities at 652 nm have a significant difference in the absence and presence of *S. aureus*. The above experimental results proved that the assay was highly specific for *S. aureus*, which was due to the highly specific affinity between an aptamer and its target on the outer surface of *S. aureus*.

3.7. Analysis of real samples

The accuracy and applicability of our proposed method were further explored by conducting three replicate analyses of *S. aureus* in model samples. As control, we used traditional culture-based method for identification of *S. aureus* in raw water. However, there is almost no bacterial colony observed in the culture plate (Fig.S8), maybe the growth of bacteria was inhibited completely during the chlorination disinfection process. So *S. aureus* spiked in these samples were monitored and the results obtained are summarized in Table 1. The average recoveries for water, urine and milk water samples were in the range of 86.5–122.3%, respectively. The relative standard derivations (RSDs) were all less than 15%. These results definitely indicate that the setup method has strong anti-interference ability for quantifying *S. aureus* in real samples.

4. Conclusion

In summary, we have developed a one-step colorimetric assay for detection of *S. aureus* simply, rapidly, sensitively, selectively and reliably. Based on target-induced shielding against the peroxidase mimicking activity of apt-Fe_3O_4/Au nanocomposites, the color change from dark blue to light blue was proportional to the concentration of *S. aureus*. Under optimal conditions, *S. aureus* can be readily detected by bare eye at a low LOD of 10 CFU mL^{-1} in 12 min with a wide linear range from 10 to 10^6 CFU mL^{-1}. Moreover, the feasibility of our approach was carried out by water samples without any pre-enrichment, separation or washing steps. Therefore, it is envisaged that our colorimetric assay will be widely used for the rapid determination of other pathogens in practical samples.

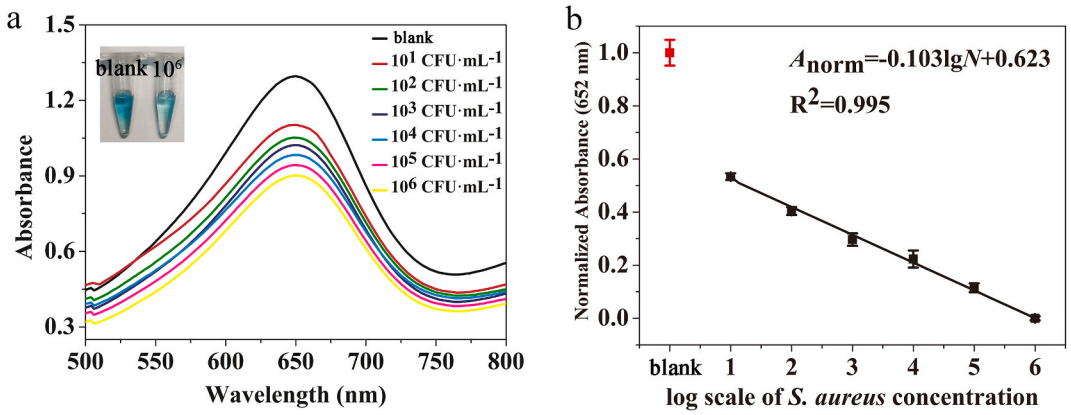

Fig. 5. a UV–Vis absorption spectra of the colorimetric detection assay in the presence of different *S. aureus* concentrations (0, 10, 10^2, 10^3, 10^4, 10^5, 10^6 CFU mL^{-1}), Inset: photograph of the colorimetric reaction with the concentration of *S. aureus* at blank and 10^6 CFU mL^{-1} **b** The calibration curve for *S. aureus* (*A*norm vs the logarithm of *S. aureus* concentration). Error bars represent the standard deviation of three replicates.

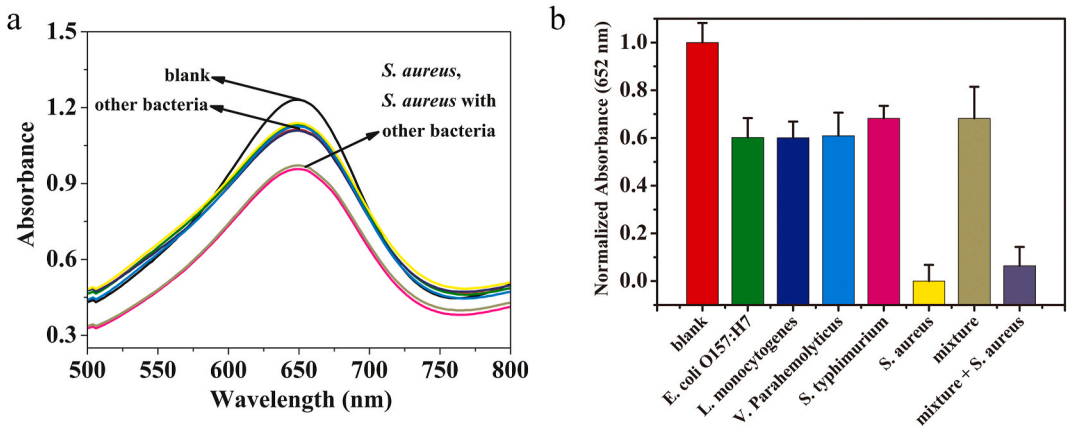

Fig. 6. Results of specificity assessment. **a** UV–Vis absorption spectra of the colorimetric detection assay in the presence of different bacterial (each at 10^6 CFU mL^{-1}). **b** Normalized absorption intensity at 652 nm in the presence of different bacteria. Error bars represent the standard deviation of three replicates.

Table 1
The recovery and RSD value of detecting *S. aureus* in spiked water and milk samples ($\bar{x} \pm s$, n = 3).

	Found (CFU·mL^{-1})	Added (CFU·mL^{-1})	Recovered (CFU·mL^{-1})	Recovery (%)	RSD (%)
Tap water 1	BDL[a]	1.0×10^2	1.1×10^2	111.3	5.8
Tap water 2	BDL[a]	1.0×10^4	0.8×10^4	87.2	5.7
Tap water 3	BDL[a]	1.0×10^6	1.1×10^6	111.1	1.4
Nanhu Lake water 1	BDL[a]	1.0×10^2	1.1×10^2	106.9	1.7
Nanhu Lake water 2	BDL[a]	1.0×10^4	1.0×10^4	102.3	1.7
Nanhu Lake water 3	BDL[a]	1.0×10^6	1.0×10^6	103.2	4.4
Industrial wastewater 1	BDL[a]	1.0×10^2	0.9×10^2	86.5	12.3
Industrial wastewater 2	BDL[a]	1.0×10^4	1.1×10^4	108.7	7.6
Industrial wastewater 3	BDL[a]	1.0×10^6	0.9×10^6	94.4	11.4
Urine sample 1	BDL[a]	1.0×10^2	1.1×10^2	113.5	10.3
Urine sample 2	BDL[a]	1.0×10^4	0.9×10^4	91.3	8.8
Urine sample 3	BDL[a]	1.0×10^6	1.2×10^6	122.3	9.6
Milk 1	BDL[a]	1.0×10^2	1.0×10^2	105.0	7.8
Milk 2	BDL[a]	1.0×10^4	0.9×10^4	96.1	5.2
Milk 3	BDL[a]	1.0×10^6	1.1×10^6	105.4	6.2

[a] *BDL* below detection limit.

Funding information

The authors thank the financial support from the National Natural Science Foundation of China (Grant No. 81872668, 81602894 and 81602895), the Education Department of Jilin Province (JJKH20180240KJ), Health commission of Jilin Province (2018Q033) and Norman Bethune Health Science Center of Jilin University (2018A05).

Compliance with ethical standards

Conflict of interest

The authors declare that they have no conflict of interest.

Credit author statement

Juan Li, Chao Zhao and Minghua Jin conceived and planned the experiments. Huiwen Zhang, Shuo Yao, Xiuling Song carried out the experiments. Huiwen Zhang, Kun Xu and Juan Wang contributed to the interpretation of the results, and wrote the manuscript. All authors discussed the results and contributed to the final manuscript.

Declaration of competing interest

The authors declare that they have no known competing financial interests or personal relationships that could have appeared to influence the work reported in this paper.

Appendix A. Supplementary data

Supplementary data to this article can be found online at https://doi.org/10.1016/j.talanta.2021.122448.

References

[1] M. Rubab, H.M. Shahbaz, A.N. Olaimat, D.H. Oh, Biosensors for rapid and sensitive detection of *Staphylococcus aureus* in food, Biosens. Bioelectron. 105 (2018) 49–57.
[2] Y.C. Chang, C.Y. Yang, R.L. Sun, Y.F. Cheng, W.C. Kao, P.C. Yang, Rapid single cell detection of *Staphylococcus aureus* by aptamer-conjugated gold nanoparticles, Sci Rep-UK 3 (2013) 1863.
[3] J. Qiao, X. Meng, Y. Sun, Q. Li, R. Zhao, Y. Zhang, Aptamer-based fluorometric assay for direct identification of methicillin-resistant *Staphylococcus aureus* from clinical samples, J Microbial Meth 153 (2018) 92–98.
[4] X. Meng, G. Yang, F. Li, T. Liang, W. Lai, H. Xu, Sensitive detection of *Staphylococcus aureus* with vancomycin-conjugated magnetic beads as enrichment carriers combined with flow cytometry, ACS Appl. Mater. Interfaces 9 (2017) 21464–21472.
[5] R. Cai, F. Yin, Z. Zhang, Y. Tian, N. Zhou, Functional chimera aptamer and molecular beacon based fluorescent detection of *Staphylococcus aureus* with strand displacement-target recycling amplification, Anal. Chim. Acta 1075 (2019) 128–136.
[6] N. Reta, C.P. Saint, A. Michelmore, B.P. Simon, N.H. Voelcker, Nanostructured electrochemical biosensors for label-free detection of water-and food-borne pathogens, ACS Appl. Mater. Interfaces 10 (2018) 6055–6072.
[7] Y. Wang, J.K. Salazar, Culture-independent rapid detection methods for bacterial pathogens and toxins in food matrices, Compr Rev Food Sci F 15 (2016) 183–205.
[8] G.A. Zelada-Guillén, J.L. Sebastián-Avila, P. Blondeau, J. Riu, F.X. Rius, Label-free detection of *Staphylococcus aureus* in skin using real-time potentiometric biosensors based on carbon nanotubes and aptamers, Biosens. Bioelectron. 31 (2012) 226–232.
[9] Y. Zhang, W. Tan, Y. Zhang, H. Mao, S. Shi, L. Duan, H. Wang, J. Yu, Ultrasensitive and selective detection of *Staphylococcus aureus* using a novel IgY-based colorimetric platform, Biosens. Bioelectron. 142 (2019) 111570.
[10] H. Sun, Y. Zu, A highlight of recent advances in aptamer technology and its application, Molecules 20 (2015) 11959–11980.
[11] P. Röthlisberger, M. Hollenstein, Aptamer chemistry, Adv. Drug Deliv. Rev. 134 (2018) 3–21.
[12] H.J. Lee, B.C. Kim, K.W. Kim, Y.K. Kim, J.B. Kim, M.K. Oh, A sensitive method to detect *Escherichia coli* based on immunomagnetic separation and real-time PCR amplification of aptamers, Biosens. Bioelectron. 24 (2009) 3550–3555.
[13] F. Chen, J. Zhou, F. Luo, A.B. Mohammed, X. Zhang, Aptamer from whole-bacterium SELEX as new therapeutic reagent against virulent *Mycobacterium tuberculosis*, Biochem Bioph Res Co 357 (2007) 743–748.
[14] R. Joshi, H. Janagama, H.P. Dwivedi, T.S. Kumar, L.A. Jaykus, J. Schefers, Selection, characterization, and application of DNA aptamers for the capture and detection of *Salmonella enterica* serovars, Mol. Cell. Probes 23 (2009) 20–28.
[15] C.L. Hamula, X.C. Le, X.F. Li, DNA aptamers binding to multiple prevalent M-types of Streptococcus pyogenes, Anal. Chem. 83 (2011) 3640–3647.
[16] J. Yuan, S. Wu, N. Duan, X. Ma, Y. Xia, J. Chen, A sensitive gold nanoparticle-based colorimetric aptasensor for *Staphylococcus aureus*, Talanta 127 (2014) 163–168.
[17] N. Duan, S.J. Wu, C. Zhu, X. Ma, Z. Wang, Y. Yu, Dual-color upconversion fluorescence and aptamer-functionalized magnetic nanoparticles-based bioassay for the simultaneous detection of *Salmonella* Typhimurium and *Staphylococcus aureus*, Anal. Chim. Acta 723 (2012) 1–6.
[18] L. Hao, H. Gu, N. Duan, S. Wu, X. Ma, Y. Xia, An enhanced chemiluminescence resonance energy transfer aptasensor based on rolling circle amplification and WS2 nanosheet for *Staphylococcus aureus* detection, Anal. Chim. Acta 959 (2017) 83–90.
[19] J. Wang, X. Wu, C. Wang, N. Shao, P. Dong, R. Xiao, Magnetically assisted surface-enhanced Raman spectroscopy for the detection of *Staphylococcus aureus* based on aptamer recognition, ACS Appl. Mater. Interfaces 7 (2015) 20919–20929.
[20] N. Tawil, E. Sacher, R. Mandeville, M. Meunier, Surface plasmon resonance detection of *E. coli* and methicillin-resistant *S. aureus* using bacteriophages, Biosens. Bioelectron. 37 (2012) 4–29.
[21] H. Guan, B. Han, D. Gong, Y. Song, B. Liu, N. Zhang, Colorimetric sensing for ascorbic acid based on peroxidase-like of GoldMag nanocomposites, Spectrochim. Acta 222 (2019) 117277.
[22] K. Ye, L. Wang, H. Song, X. Li, X. Niu, Bifunctional MIL-53 (Fe) with pyrophosphate-mediated peroxidase-like activity and oxidation-stimulated fluorescence switching for alkaline phosphatase detection, J. Mater. Chem. B 7 (2019) 4794–4800.
[23] Z. Zhang, G. Xu, L. Xie, Y. Guan, Colorimetric immunoassay for human chorionic gonadotropin by using peroxidase-mimicking MnO_2 nanorods immobilized in microplate wells, Mikrochim. Acta 186 (2019) 581.
[24] R. Das, A. Dhiman, A. Kapil, V. Bansal, T.K. Sharma, Aptamer-mediated colorimetric and electrochemical detection of Pseudomonas aeruginosa utilizing peroxidase-mimic activity of gold NanoZyme, Anal. Bioanal. Chem. 411 (2019) 1229–1238.
[25] J. Zhu, X. Peng, W. Nie, Y. Wang, J. Gao, W. Wen, Hollow copper sulfide nanocubes as multifunctional nanozymes for colorimetric detection of dopamine and electrochemical detection of glucose, Biosens. Bioelectron. 141 (2019) 111450.
[26] L. Gao, J. Zhuang, L. Nie, J. Zhang, Y. Zhang, N. Gu, Intrinsic peroxidase-like activity of ferromagnetic nanoparticles, Nat. Nanotechnol. 2 (2007) 577.
[27] K. Fan, H. Wang, J. Xi, Q. Liu, X. Meng, D. Duan, Optimization of Fe_3O_4 nanozyme activity via single amino acid modification mimicking an enzyme active site, Chem. Commun. 53 (2017) 424–427.
[28] P. Zan, C. Yang, H. Sun, L. Zhao, Z. Lv, Y. He, One-pot fabricating Fe_3O_4/graphene nanocomposite with excellent biocompatibility and non-toxicity as a negative MR contrast agent, Colloids Surf. B Biointerfaces 145 (2016) 208–216.
[29] H. Liu, L. Zhu, H. Ma, J. Wen, H. Xu, Y. Qiu, Copper (II)-coated Fe_3O_4 nanoparticles as an efficient enzyme mimic for colorimetric detection of hydrogen peroxide, Mikrochim. Acta 186 (2019) 518.
[30] Y. Li, J. Liu, Y. Fu, Q. Xie, Y. Li, Correction to: magnetic-core@dual-functional-shell nanocomposites with peroxidase mimicking properties for use in colorimetric and electrochemical sensing of hydrogen peroxide, Mikrochim. Acta 186 (2019) 456.
[31] C. Zhang, C. Wang, R. Xiao, L. Tang, J. Huang, D. Wu, S. Liu, Y. Wang, D. Zhang, S. Wang, X. Chen, Sensitive and specific detection of clinical bacteria via vancomycin-modified Fe_3O_4@Au nanoparticles and aptamer-functionalized SERS tags, J. Mater. Chem. B 6 (2018) 3751–3761.
[32] W.W. Wang, X. Han, L.Q. Chu, Polyadenine-Mediated immobilization of aptamers on gold substrate for direct detection of bacterial pathogens, Anal. Sci. 35 (2019) 967–972.
[33] A.G. Bozkurt, G.G. Buyukgoz, M. Soforoglu, U. Tamer, Z. Suludere, I.H. Boyaci, Alkaline phosphatase labeled SERS active sandwich immunoassay for detection of *Escherichia coli*, Spectrochim. Acta Mol. Biomol. Spectrosc. 194 (2018) 8–13.
[34] C. Zhang, Y. Gao, N. Yang, T. You, H. Chen, P. Yin, Direct determination of the tumor marker AFP via silver nanoparticle enhanced SERS and AFP-modified gold nanoparticles as capturing substrate, Mikrochim. Acta 185 (2018) 90.
[35] K. Fu, Y. Zheng, J. Li, Y. Liu, B. Pang, X. Song, Colorimetric immunoassay for rapid detection of *Vibrio parahemolyticus* based on Mn^{2+} mediates the assembly of gold nanoparticles, J. Agric. Food Chem. 66 (2018) 9516–9521.
[36] R. Ravisankar, S. Kiruba, P. Eswaran, G. senthilkumar, A. chandrasekaran, Mineralogical characterization studies of ancient potteries of tamilnadu, India by FT-IR spectroscopic technique, J Chem-ny 7 (2010) S185–S190.
[37] L. Aljerf, R. Nadra, Developed greener method based on MW implementation in manufacturing CNFs, Int. J. Nanomanufacturing 15 (2019) 269–289.
[38] S. Jampasa, P. Lae-Ngee, K. Patarakul, N. Ngamrojanavanich, O. Chailapakul, N. Rodthongkum, Electrochemical immunosensor based on gold-labeled monoclonal anti-LipL32 for leptospirosis diagnosis, Biosens. Bioelectron. 142 (2019) 111539.